Study of Crystallization Processes in Ethylene−Styrene Copolymers by Conventional DSC and Temperature-Modulated Calorimetry: Linear Polyethylene and Low Styrene Content Copolymers

Zhenyu Huang,[†] Hervé Marand,*[,†] Wilson Y. Cheung,[‡] and Martin Guest[‡]

Department of Chemistry, Virginia Polytechnic Institute and State University, Blacksburg, Virginia 24061-0212 and Polyolefin Division, The Dow Chemical Company, Freeport, Texas 77541

Received March 25, 2004; Revised Manuscript Received September 8, 2004

ABSTRACT: Using a combination of differential scanning calorimetry and quasi-isothermal temperature-modulated calorimetry, we investigated the temporal evolutions of the melting temperature, degree of crystallinity, and excess heat capacity during crystallization of linear polyethylene and low styrene content ethylene−styrene copolymers. Describing isothermal crystallization as the succession of three stages (primary, mixed and secondary crystallization stages), we established the following correlations: (1) the evolution of the melting temperature with time parallels that of the degree of crystallinity, (2) the excess heat capacity increases linearly with degree of crystallinity during the primary stage, reaches a maximum during the mixed stage, and decays during the secondary stage, (3) the rate of decay of the excess heat capacity parallels the rate of secondary crystallization, and (4) the rates of shift of the melting temperature and decay of the excess heat capacity lead to apparent activation energies that are very similar to these reported for the crystal α_c relaxation by solid-state NMR, dynamic mechanical, and dielectric spectroscopies. Strong correlations in the time domain for secondary crystallization by lamellar thickening and evolution of the excess heat capacity suggest that the reversible crystallization/melting phenomenon is associated with molecular events in the melt−crystal fold interfacial region. Specifically, we conclude that the excess heat capacity observed during the high-temperature crystallization of linear polyethylene and low styrene content copolymers is most likely to originate from the segmental processes in the crystal/melt fold region that have been discussed by Fischer, Mansfield, and Strobl. These studies also provide preliminary indications that the excess heat capacity observed during crystallization at lower temperatures in the case of ethylene copolymers of high comonomer content is consistent with the lateral surface model proposed by Wunderlich.

Introduction

It is well known that polymers, in contrast with most small molecules, require large supercoolings to crystallize at a measurable rate under quiescent conditions. The actual magnitude of the supercooling depends on the mode of nucleation (heterogeneous, homogeneous, and self-nucleation). While 10−30 K supercoolings are typical of heterogeneous nucleation, 50−140 K supercoolings have been reported for the homogeneous nucleation of linear polymeric liquids. The resulting crystallites usually melt at temperatures significantly above their crystallization temperature.[1] Thus, the temperature dependence of the degree of crystallinity in polymers usually displays a significant hysteresis, and irreversibility is a common feature of the crystallization−melting behavior of polymers. However, a number of calorimetric experiments using the recently developed temperature-modulated DSC technique suggest the existence of some reversibility in the crystallization/melting process for a few polymers.[2−19] TMDSC experiments indicate that the measured reversing heat capacity is larger than the baseline heat capacity, calculated as the weight average of the liquid and crystal phase heat capacities assuming a simple two-phase model. The difference between reversing and baseline heat capacities is called the excess reversing heat capacity or, simply, the excess heat capacity. Contributions to the excess heat capacity arise from reversible crystallization and melting processes that do not require nucleation, supercooling, or superheating and from any nonreversing processes occurring on the time scale of the temperature modulation.

The possible mechanisms associated with these reversible crystallization/melting processes are still being debated. Strobl et al.[8,14,20] proposed that the reversible crystallization and melting occur on the fold surface of crystallites. Their argument is based on Fischer's assumption[21] of a local equilibrium or force balance between stretched loops or tie chains in the interlamellar amorphous region and crystal stems in lamellae. The former tend to relax by drawing chains out of the crystal, and the latter tend to draw the loop into the crystal. Using Fischer's hypothesis, Mansfield et al.[22,23] and Strobl et al.[20] derived analytical expressions accounting for reversible changes in the amorphous layer thickness in the case of linear polyethylene.[24] The transport of polymer segments between the amorphous and the crystal phases may be reversible under the experimental conditions of temperature modulation if a mechanism, such as sliding diffusion, is available for segmental motion within the crystalline phase. The latent heat exchanged during this reversible process would then be the primary contributor to the excess heat capacity measured by temperature-modulated calorimetry. Hu et al.[8] found that the magnitude of the excess heat capacity is associated with the extent to which chain segments undergo sliding diffusion in the crystal phase, which, on the other hand, leads to lamellar thickening. In polymers such as PE or PEO, which should display relative ease of sliding diffusion, consid-

* To whom correspondence should be addressed.
[†] Virginia Polytechnic Institute and State University.
[‡] The Dow Chemical Company.

10.1021/ma049411g CCC: $27.50
Published on Web 12/04/2004

erable excess heat capacity is observed. In contrast, polymers such as s-PP, which are believed to exhibit little if any sliding diffusion in the crystal phase, show almost no excess heat capacity.[8] Thus, the excess heat capacity can be related to chain mobility in the crystalline phase. In turn, this observation provides support for the important role of segmental transport at the melt−crystal fold interface in the reversible crystallization/melting process. Further support for the fold surface model has also been obtained by time-resolved, temperature-modulated WAXD/SAXS experiments.[15]

However, one should note that this model can only explain the existence of excess heat capacity in the high-temperature region where segmental relaxation in the crystalline phase is relatively rapid and local thermodynamic equilibrium can be reached at the crystal−melt fold surface on the time scale of the temperature modulation. At lower temperatures, as the frequency of segmental jumps in the crystalline phase decreases dramatically, much longer relaxation times must be associated with any reorganization of the crystal−melt interphase. For instance, a four-decade increase in the relaxation time associated with segmental jump is inferred from solid-state NMR measurements[25] for linear PE between 100 °C and room temperature. This kinetic barrier inhibits the segmental transport at the crystal−liquid fold interface on the time scale of the temperature modulation. Furthermore, in ethylene/styrene copolymers, the presence of short branches likely to accumulate near the fold surface of lamellae will hinder and eventually inhibit the sliding diffusion of segments in the crystalline phase. Therefore, we suggest that the excess heat capacity observed in the low-temperature region cannot be associated with the sliding diffusion mechanism and requires an alternative explanation.

Wunderlich et al. proposed a different model that considers the attachment and detachment of segments on the lateral surface of crystallites as the source of reversible crystallization and melting in polymers.[3] They investigated a series of materials including PET, PEO, it-PP, ethylene/1-octene copolymers, n-paraffins, and PE's of varying molar mass. They suggested that the reversibility increases with increasing the lateral specific surface area of the crystals.[13,17] Advocates of the fold surface mechanism have rejected this model because they believe that recrystallization during the cooling stage of the temperature modulation should lead to thicker lamellae that are more difficult to melt in the subsequent heating stage.[15]

In the present study, the reversible melting and crystallization behavior of a linear polyethylene fraction and of some low styrene content ethylene random copolymers will be investigated using conventional DSC and temperature-modulated calorimetry. On the basis of our results of the evolution of the melting temperature, degree of crystallinity, and excess heat capacity during isothermal crystallization, we attempt to correlate the evolution of the excess heat capacity with time with the increase in topological constraints resulting from the secondary crystallization, thought to be of the lamellar thickening type in the case of linear polyethylene and low styrene content copolymers.

Experimental Section

Materials. A series of statistical ethylene copolymers with composition ranging from 0.35 to 3.4 mol % styrene were used as received from the Dow Chemical Co. Their molecular characteristics are shown in Table 1. These materials (trade name INDEX) were synthesized using the Insite technology and are called "pseudorandom ethylene/1-styrene interpolymers" (ESI) due to the absence of successive head-to-tail styrene insertions. Hence, they are appropriately described as random copolymers of ethylene units and ethylene/styrene dyads. The behavior of these materials was compared to that of a narrow molar mass distribution linear polyethylene sample (SRM1184a) obtained from NIST.

Table 1. Molecular Characteristics of Linear Polyethylene and Ethylene−Styrene Copolymers

sample	wt % styrene	M_w (g/mol)	polydispersity (M_w/M_n)	mol % styrene
PE-119K	0	119 600	1.19	0
ESI-0.35	1.3	168 000	2.0	0.35
ESI-1.9	6.8	160 200	2.3	1.9
ESI-3.4	11.6	175 100	2.2	3.4

Differential Scanning Calorimetry (DSC). The calorimetric experiments were performed in a Pyris model Perkin-Elmer differential scanning calorimeter operated under purified nitrogen with an ice−water bath heat sink. Calibrations of the temperature scale and latent heat were described in the preceding paper of this series.[29]

Studies of the melting behavior were carried out after isothermal crystallization using a heating rate of 10 K/min. Films of copolymers were prepared by successive compression molding at 165 °C under a pressure of 1 MPa in a Carver laboratory press under dry nitrogen atmosphere for 5 min and quenching into an ice−water mixture. To minimize the effect of temperature gradients on the melting trace and enhance the resolution in thermograms exhibiting multiple melting peaks, sample mass and thickness were kept relatively low (ca. 2.0 ± 0.2 mg and 50−100 μm, respectively).

Melting temperatures reported here correspond to peak temperatures of endothermic transitions. Heats of fusion of isothermally crystallized samples were estimated through a previously described subtraction method.[29]

Temperature-Modulated Calorimetry. The temperature-modulated calorimetric experiments were performed with the same equipment as the classical DSC work discussed above. The saw-tooth mode of modulation was employed under quasi-isothermal conditions. Experimental reversing heat capacities (C_p^{rev}(exp)) were calculated using eq 1 from the heat flow (A_{HF}) and temperature (A_{Ts}) amplitudes and subsequently corrected by extrapolation to zero frequency, following the procedure (eq 2) described by Androsch[26]

$$C_p^{rev}(\exp) = A_{HF}/\omega A_{Ts} \quad (1)$$

$$[1/C_p^{rev}(\exp)]^2 = [1/C_p^{rev}(\mathrm{corr})]^2(1 + \tau^2\omega^2) \quad (2)$$

The corrected reversing heat capacity C_p^{rev}(corr) was further calibrated using a sapphire standard. In the case of a material such as sapphire, which exhibits neither irreversible nor reversible latent heat effects in the temperature range of interest in this work, C_p^{rev} represents the true material heat capacity. However, in the range of temperatures between T_g and T_m, the reversing heat capacity, C_p^{rev} of a semicrystalline polymer may display contributions from reversible latent heat effects. It is therefore useful to define an excess reversing heat capacity, C_p^{exc}, to represent the difference between the corrected reversing heat capacity, C_p^{rev}, and the materials true heat capacity, C_p.

In the present study, C_p was calculated for each copolymer as a function of temperature using a simple rule of mixing as shown by eq 3.

$$C_p(\mathrm{ESI}) = X_c C_p^c(\mathrm{PE}) + (1 - X_c - \phi)C_p^a(\mathrm{PE}) + \phi C_p^a(\mathrm{PS}) \quad (3)$$

In this equation ϕ represents the weight fraction of styrene

and X_c the weight fraction crystallinity, estimated from DSC results and accounting for the temperature dependence of the heat of fusion for a perfect polyethylene crystal. The quantities C_p^c(PE), C_p^a(PE), and C_p^a(PS) represent the specific heat capacities of polyethylene's crystal and liquid phases and polystyrene liquid phase, which can be obtained from the ATHAS data bank.[27] The excess (reversing) heat capacity of ethylene copolymers is then obtained by subtraction of C_p from the experimentally determined C_p^{rev} value. To derive eq 3 we assumed (1) a two-phase model (no interphase or rigid amorphous phase), (2) exclusion of the styrene units from the crystalline regions (polyethylene), and (3) representation of the specific heat capacity for the amorphous phase of ethylene−styrene copolymers by the weight-average specific heat capacity of the corresponding homopolymers. While the latter assumption may be viewed with skepticism, quantitative agreement between calculated and experimentally measured values of C_p in the melt state for ESI-3.4 suggests that this approximation is indeed quite acceptable.

Although the temperature-modulated technique presents many advantages over conventional DSC, one should be aware that experimental results obtained under temperature modulation could exhibit artifacts arising from nonlinearity and/or heat transfer effects. It is therefore imperative to choose appropriately those experimental parameters that affect the linearity and stationarity conditions (e.g., sample thickness, temperature amplitude, underlying heating rate, and modulation frequency). The theory for temperature-modulated differential scanning calorimetry is still in development, and great caution should be exercised during both experimental design and data interpretation, especially for experiments carried out during cooling or heating.

In the present study material heat capacities were calibrated using a sapphire standard. The heat capacity of sapphire was first measured at different temperatures over a range of frequencies (0.003−0.05 Hz) and extrapolated to zero frequency using eq 2. The extrapolated values were then compared with the literature values[28] to obtain correction factors at different temperatures (typically in the range of 1.08−1.17). For heat capacity measurements with ethylene copolymers, the time constant, $\tau = 1.23$ s, was estimated using eq 2 at 393 K for ESI 3.4. As indicated above, corrected experimental copolymer heat capacities match very closely (less than a few percent) these calculated from the ATHAS data bank.[27] The same time constant ($\tau = 1.23$ s) was used in the analysis of the quasi-isothermal data recorded during crystallization at different temperatures. We assumed τ to be constant in the narrow range of temperatures considered (358−403 K). Even if this assumption is not rigorously justified, it does not compromise in any way the KWW analysis presented below. In all cases, the quasi-isothermal experiments were performed using a temperature amplitude $A_{Ts} = 0.8$ K and a period equal to 48 s.

Results

In the first section we discuss the evolution of DSC melting traces recorded after isothermal crystallization for different times. In the second section we focus on the results of quasi-isothermal temperature-modulated calorimetric experiments. The correspondence between results from DSC and temperature-modulated calorimetry is highlighted as appropriate.

1. Study of the Melting Behavior after Isothermal Crystallization by DSC. *1.1. DSC Melting Trace.* Figure 1a−h represents DSC melting traces for linear polyethylene and ESI copolymers with styrene ranging from 0.35 to 3.4 mol % after isothermal crystallization for different times. For each sample a sufficiently high crystallization temperature was selected to ensure that both primary and secondary crystallization processes are observed in detail (Figure 1a, c, e, g). In addition, secondary crystallization was also investigated at lower temperatures, where primary crystallization is either completed at these temperatures after relatively short times or during cooling (Figure 1b, d, f, h).

For both the linear polyethylene fraction PE-119K and the ESI-0.35 copolymer, single melting peaks are observed, suggesting that only one type of crystallite is formed at both high and low crystallization temperatures. In both cases, the peak melting temperature shifts to higher value with increasing crystallization time.

With a further increase in the styrene content, multiple melting behavior sets in. In the case of ESI-1.9, two endotherms are easily identified at both $T_x =$ 114 and 105 °C, especially at short crystallization times. For $T_x = 114$ °C, low and high endotherms develop at approximately the same rate during the early stage of crystallization. While the area of the high endotherm grows at a much reduced rate after a certain crystallization time, the area of the low endotherm continues to increase. For $T_x = 105$ °C, both endotherms shift to higher temperature with longer crystallization times. For this crystallization temperature, the low endotherm displays again a much larger change in magnitude than the high endotherm for long crystallization times.

For higher styrene content copolymers, such as ESI-3.4, a similar multiple melting behavior is also observed. However, in this case three endotherms are observed for crystallization at high temperatures. In the subsequent paper of this series, where we focus on the crystallization and melting behavior of high styrene content copolymers, we show that the upper two endotherms are associated with a melting−recrystallization−remelting process. Hence, only the lowest two endotherms provide information on the thermal stability of crystals formed under isothermal crystallization conditions. We note in this case that only a slight upward shift in the location of the intermediate endotherm is observed at high crystallization temperature and for long times. In contrast with observations reported above for lower styrene content copolymers, the enthalpy and peak temperature associated with the intermediate endotherm of ESI-3.4 eventually become independent of time at low crystallization temperature.

We now focus on the evolution of the peak melting temperature for samples exhibiting a single endotherm (PE-119K and ESI-0.35) and for samples exhibiting multiple endotherms (ESI-1.9 and ESI-3.4).

1.2. Evolution of Melting Temperature with Crystallization Time. For high crystallization temperatures, ESI-0.35 exhibits a similar melting behavior to that reported previously for PE-119K.[29] In this case the melting temperature increases in a sigmoidal fashion with the logarithm of time (see Figure 2). We showed in that study[29] that the evolution of the melting temperature and degree of crystallinity during isothermal crystallization are correlated. This observation suggested that these phenomena can be viewed as the consequences of the same underlying process, i.e., lamellar thickening.[29] The sigmoidal shape led us to conclude that crystallization can be roughly divided into three stages. While the first and last stages correspond to "approximately" pure primary and secondary crystallization processes, respectively, the intermediate or mixed stage is associated with time scales over which both primary and secondary crystallization significantly contribute to the rise in crystallinity. Characteristic features of the secondary process will therefore be

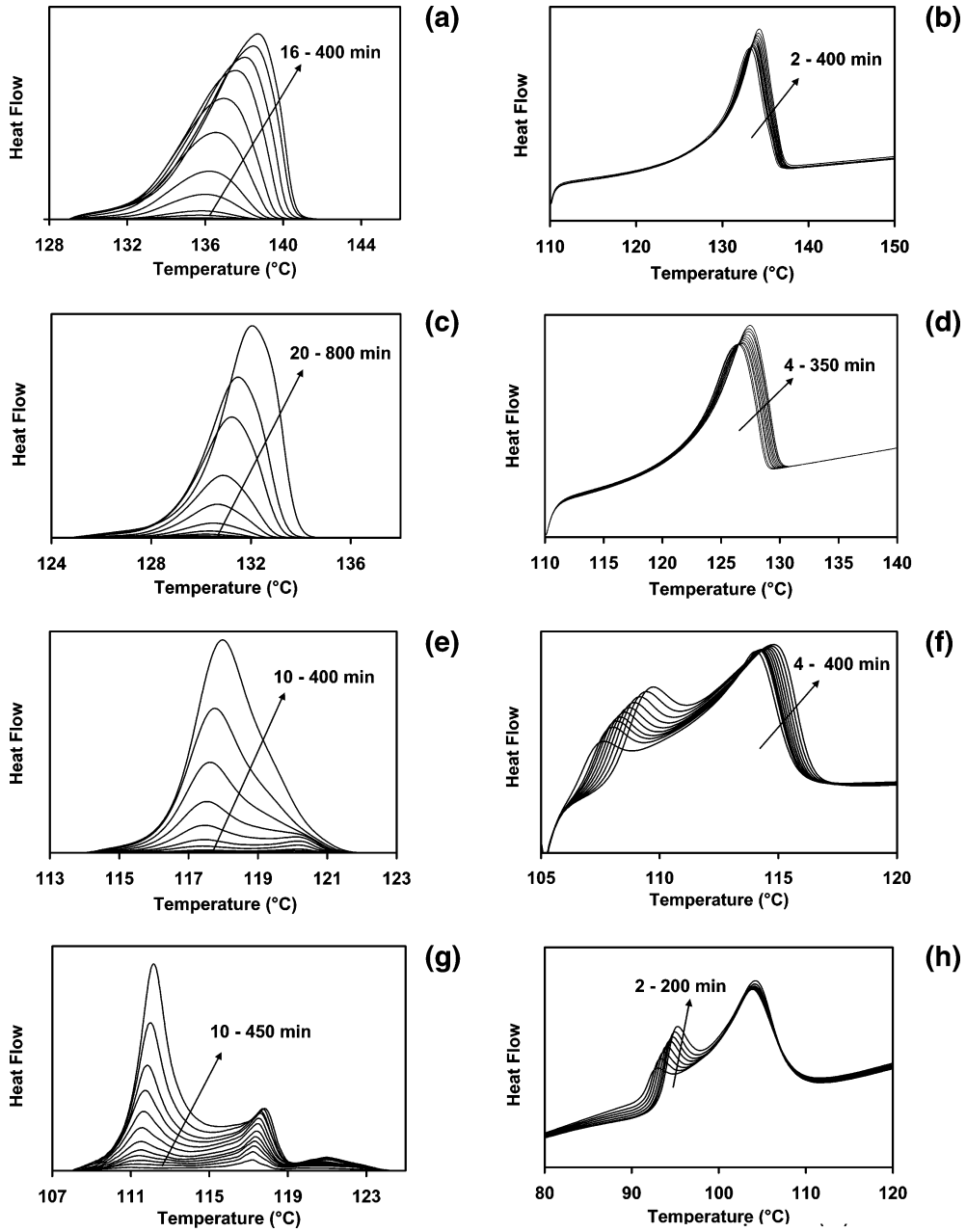

Figure 1. Evolution of the experimental melting trace with crystallization time for PE-119K at (a) $T_x = 129$ °C and (b) $T_x = 110$ °C, for ESI-0.35 at (c) $T_x = 124.7$ °C and (d) $T_x = 110$ °C, for ESI-1.9 at (e) $T_x = 114$ °C and (f) $T_x = 105$ °C, and for ESI-3.4 at (g) $T_x = 108$ °C and (h) $T_x = 90$ °C (range of crystallization times as indicated).

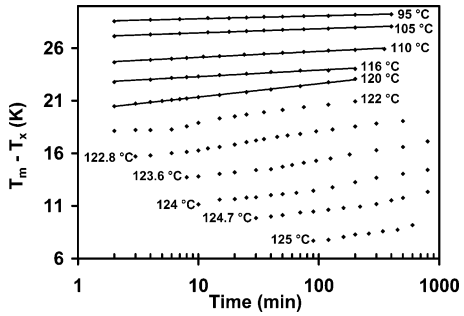

Figure 2. Evolution of the difference between melting and crystallization temperatures as a function of residence time at the indicated temperatures for ESI-0.35. Data were arbitrarily shifted along the temperature axis for the sake of clarity.

obtained from the evolution of the melting temperature after crystallization for long times. Consequently, in cases where the sigmoidal behavior is observed, we define $B(T_x)$, the rate of shift of the melting temperature with crystallization time as the slope of $T_m(t)$ vs $\log(t)$ at long times.

For lower crystallization temperatures plots of the melting temperature vs logarithm of time are linear, as shown in Figure 2 for ESI-0.35. This is similar to the behavior reported previously for PE-119K.[29] It is noted in these cases ($T < 120$ °C for ESI-0.35 and $T < 122$ °C for PE-119K) that primary crystallization reaches completion during the cooling process. In these latter cases only the secondary crystallization process can be considered to occur for the most part under isothermal conditions.

For the stage of crystallization where the melting temperature varies linearly with the logarithm of crystallization time, we can write

$$T_m = T_x + A(T_x) + B(T_x)\log(t_x) \qquad (4)$$

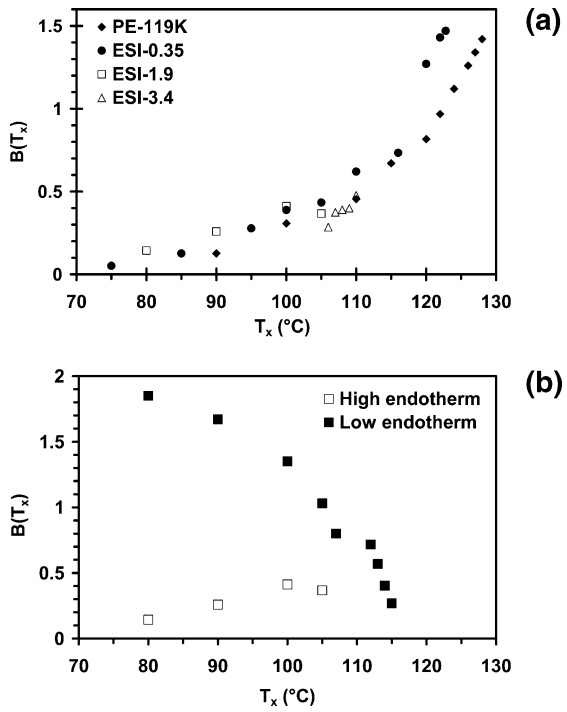

Figure 3. Melting temperature shift rate $B(T_x)$ as a function of crystallization temperature for (a) PE-119K, ESI-0.35, ESI-1.9, and ESI-3.4 (data for ESI-1.9 and ESI-3.4 are inferred from their high endotherm) and (b) for ESI-1.9, calculated for the low and the high endotherms.

where $B(T_x)$ is defined above and should be a function of comonomer content and crystallization temperature. Figure 3a shows the evolution of $B(T_x)$ with temperature for linear PE and for a series of ethylene−styrene copolymers. In all cases $B(T_x)$ is observed to increase slowly at low temperature and faster at higher temperature. For crystallization of ESI-1.9, $B(T_x)$ displays different behaviors for the low and high endotherms (see Figure 3b). $B(T_x)$ increases slightly with temperature for the high endotherm and decreases with temperature for the low endotherm. Overlap between the low and high endotherms for ESI-1.9 samples crystallized at high temperature prevents the determination of $B(T_x)$ for T_x above 106 °C. Finally, we also note that below ca. 110−115 °C copolymers of different compositions (between 0 and 3.4 mol % styrene) follow the same $B(T_x)$ curve as the homopolymer.

1.3. Correspondence between Melting Temperature and Crystallinity. We already alluded to the correlation between the evolution of the melting temperature and that of the degree of crystallinity during isothermal crystallization.[29] In support of this assertion, we will see below that the end of the first stage in the sigmoidal evolution of the melting temperature correlates very well with the time at which departure from the Avrami behavior is observed. Traditionally, the Avrami equation has been used to characterize the evolution of crystallinity during the initial stage (primary stage) of isothermal crystallization

$$X_c(t) = X_c(\infty)\,[1 - \exp(-kt^n)] \qquad (5)$$

where $X_c(t)$ is the degree of crystallinity at time t and $X_c(\infty)$ is the limiting degree of crystallinity at the end of primary crystallization. The degree of crystallinity, $X_c(t)$, is calculated here from the ratio $\Delta H_f(t)/\Delta H_f^0$, where $\Delta H_f(t)$ and ΔH_f^0 are the heat of fusion after crystallization for time t and the thermodynamic heat of fusion for a perfect crystal, respectively. k is the primary crystallization rate constant, and n, the Avrami exponent, is related to the geometry of crystal superstructure and type of nucleation and growth. Linearity in a plot of $\ln[-\ln(1 - X_c(t)/X_c(\infty))]$ vs $\ln t$ can then be used to infer that a single crystallization mechanism is at play (here, primary crystallization). Deviation from linearity in such plots has often been used to indicate that secondary crystallization within the existing semicrystalline morphology is starting to contribute significantly to the overall increase in crystallinity.[30]

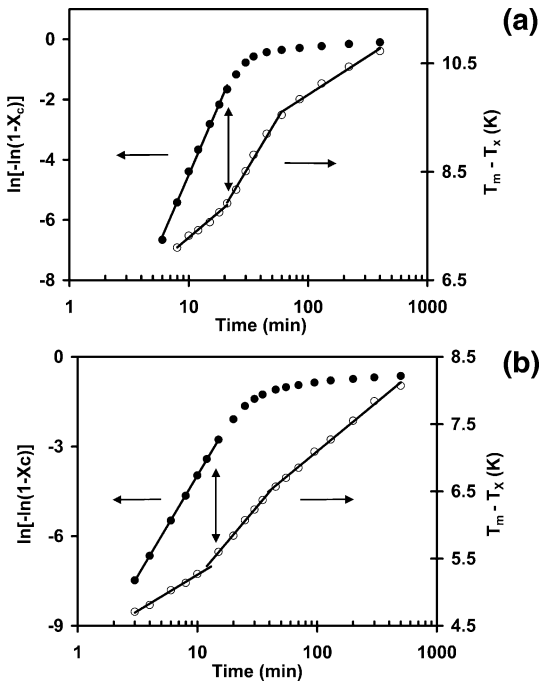

Figure 4. Correspondence between the first stage of the melting temperature evolution and the linear region of the Avrami plot for (a) PE-119K at T_x = 128 °C and (b) ESI-0.35 at T_x = 122.8 °C.

Examination of Figure 4a for PE-119K (T_x = 128 °C) and Figure 4b for ESI-0.35 (T_x = 122.8 °C) indeed suggests that the first stage in the evolution of the melting temperature corresponds to the linear part of the Avrami plot (primary crystallization) while the third stage is associated with secondary crystallization. The same conclusion was reached for all crystallization experiments where the sigmoidal behavior was observed.

2. Quasi-isothermal Temperature-Modulated Calorimetry. *2.1. Evolution of the Excess Heat Capacity during Crystallization.* In this section we report the results from quasi-isothermal experiments carried out over a wide temperature range as shown in Figure 5. The excess heat capacity increases during the initial stage of crystallization at high temperature (sigmoidal shape), reaches a maximum, and subsequently decays over very long periods of time. At lower temperature, where primary crystallization reaches completion during cooling, only the decay stage is observed.

Here, we attempt to correlate the temporal evolutions of the excess heat capacity, degree of crystallinity, and resulting melting behavior. We note, first, that the onset of decay for the excess heat capacity at high crystallization temperature approximately corresponds to the beginning of the third stage in the evolution of the melting temperature as shown in Figure 6 for the case

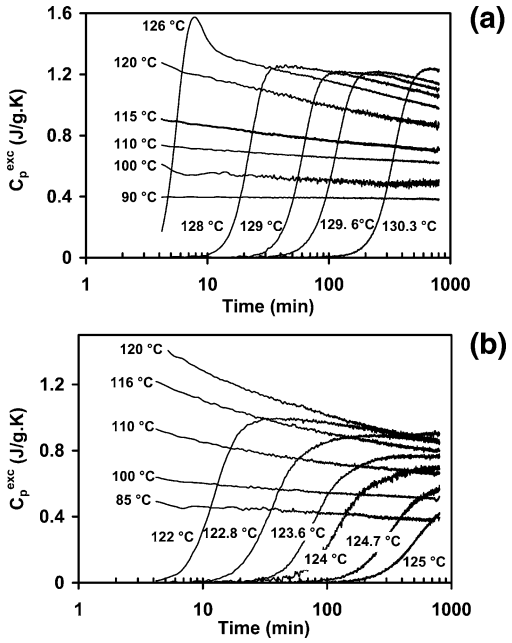

Figure 5. Evolution of the excess heat capacity with time during quasi-isothermal experiments for (a) PE-119K and (b) ESI-0.35 (for the indicated crystallization temperatures).

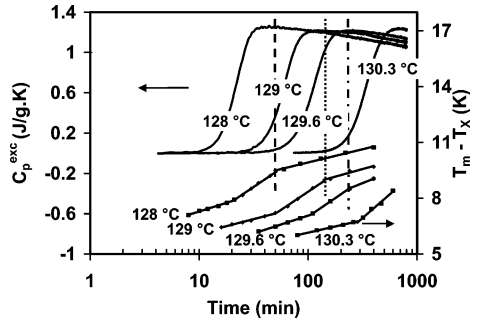

Figure 6. Correspondence between the three stages of the melting temperature evolution and the decay of excess heat capacity (for the indicated crystallization temperatures).

of PE-119K (T_x = 128, 129, and 129.6 °C). For T_x = 130.3 °C, the third stage in the T_m curve and the decay in excess heat capacity curve are expected to be observed for longer crystallization times. ESI-0.35 shows a similar behavior. Examination of Figures 4 and 6 indicates that the decay of the excess heat capacity is a feature of secondary crystallization in the case of linear polyethylene and low styrene content copolymers. Similar conclusions were reached earlier on by Toda et al.[2]

2.2. Correlation between Excess Heat Capacity and Crystallinity. Examination of Figure 5 suggests that the development of the excess heat capacity mirrors that of the crystallinity during the initial stage of isothermal crystallization. Similar observations have been reported by Toda et al.[2] To ascertain whether this comparison has any merit, we show the changes in excess heat capacity and crystallinity as a function of time on the same plot for ESI-0.35 (Figures 7a). The relative scales for C_p^{exc} and X_c were chosen so as to superpose these two quantities as best as possible from the onset of crystallization. Examination of Figure 7a and b indicates that superposition of C_p^{exc} and X_c is observed up to a time, t_x*, characteristic of the end of primary crystallization. This indicates that the excess heat capacity is proportional to the degree of crystallinity during primary crystallization in the free melt.

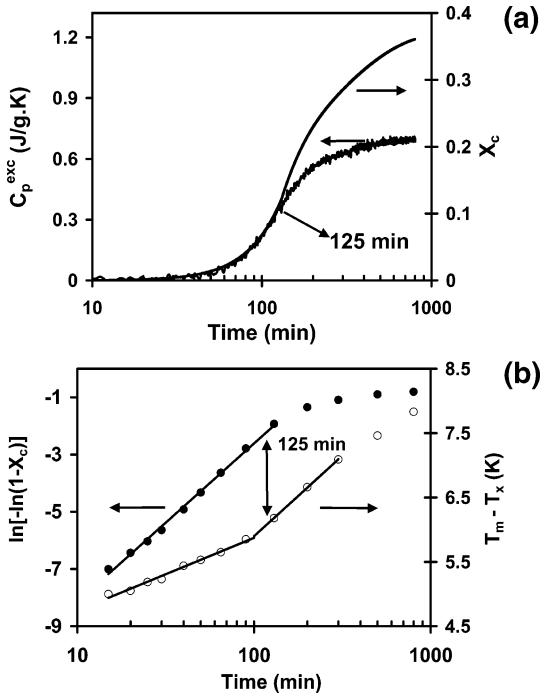

Figure 7. Correlations between excess heat capacity, crystallinity, and melting temperature during quasi-isothermal or isothermal crystallization of ESI-0.35 at T_x = 124 °C: (a) correlations between the excess heat capacity and the degree of crystallinity; (b) correlations between the evolution of the melting temperature and that of the degree of crystallinity.

2.3. Characterization of the Decay of Excess Heat Capacity−KWW Analysis. In the preceding sections we reported the evolution of the excess heat capacity with time during isothermal crystallization and showed that this quantity is correlated with the evolution of the degree of crystallinity and the melting temperature. In this section we show that valuable information can be obtained from a quantitative analysis of the time dependence of the excess heat capacity during secondary crystallization. Anticipating from previous studies that secondary crystallization by lamellar thickening is somehow related to the existence of a crystal α_c relaxation process, we attempted to fit the excess heat capacity decay curve with the Kohlrausch−Williams−Watts (KWW) equation[31]

$$C_p^{exc}(t) = C_p^{exc}(\infty) + [C_p^{exc}(0) - C_p^{exc}(\infty)] \exp[-(t/\tau)^{\beta}] \quad (6)$$

where $C_p^{exc}(0)$ and $C_p^{exc}(\infty)$ are the upper and lower bounds of the excess heat capacity at time zero and infinity, respectively, τ is a characteristic relaxation time, and β is an exponent characterizing the heterogeneity of the relaxation process (β = 1 implies a single relaxation time process, while β < 1 suggests a distribution of relaxation times). The KWW equation has often been used to describe segmental relaxation in amorphous polymers. In the present case, the decay of excess heat capacity arises from irreversible effects associated with the decrease in the number of amorphous segments able to undergo reversible crystallization−melting processes. The decrease in excess heat capacity should be traced either directly to secondary crystallization by lamellar thickening or to an increase in constraints experienced by amorphous segments at the melt−crystal interfaces.

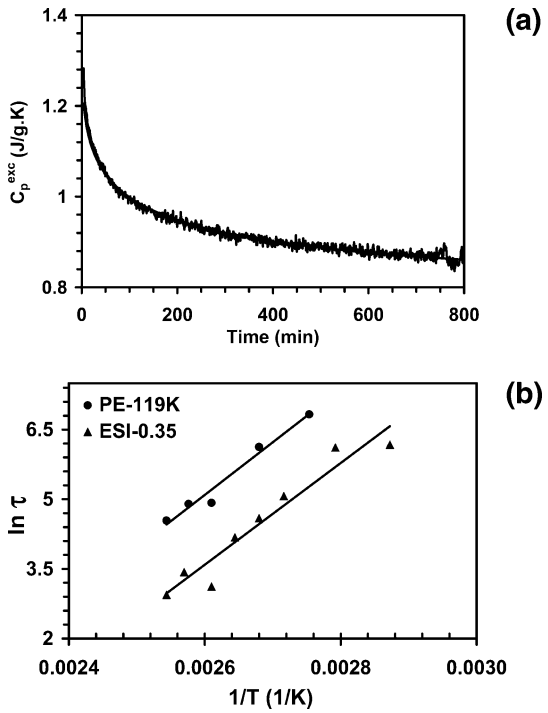

Figure 8. KWW analysis for the evolution of the excess heat capacity with time. (a) Experimental $C_p^{exc}(t_x)$ data and best fit to the KWW equation for PE-119K at $T_x = 120$ °C. (b) Arrhenius plot of characteristic time, τ, inferred from the KWW equation for PE-119K and ESI-0.35. The apparent activation energies, given in Table 3, are calculated from the slopes.

The application of the KWW equation to the decay of C_p^{exc} must be considered a priori phenomenological. We note that the decay of excess heat capacity is very well fitted by the KWW equation (Figure 8a).

To estimate the characteristic relaxation time, τ, we prepared a plot of $\ln\{-\ln[(C_p^{exc}(t) - C_p^{exc}(\infty))/(C_p^{exc}(0) - C_p^{exc}(\infty))]\}$ vs $\ln t$. The values for $C_p^{exc}(\infty)$ are obtained by minimization of the variance associated with the linear regression. It is found that τ increases with decreasing crystallization temperature for both PE-119K and ESI-0.35 in the range from 85 to 110 °C. Apparent activation energy for the underlying relaxation process is obtained by plotting $\ln \tau$ vs $1/T$ (Figure 8b). Apparent activation energies of 94 ± 9 and 91 ± 10 kJ/mol are inferred from these plots for PE-119K and ESI-0.35, respectively.

One must be aware, however, that this approach is unlikely to work in situations where secondary crystallization occurs simultaneously by lamellar thickening and through the formation of small secondary crystals. As will be discussed in the next paper of this series, the latter process will contribute in a different way to the evolution of the excess heat capacity during isothermal crystallization.

Discussion

One of the major objectives of this study is to explain the correlations between the evolution of the degree of crystallinity, the melting temperature, and the excess heat capacity. Another important objective is to understand the origin of the excess heat capacity (reversible crystallization and melting) and to account for its dependence on temperature and comonomer content. Finally, a further outcome of the present studies should be a better overall understanding of the secondary crystallization process.

To understand both the origin of the excess heat capacity and its systematic evolution during secondary crystallization, we need to clarify the origin of the secondary crystallization process and discuss how experimental conditions and polymer microstructure affect its mechanism.

Two broad categories of models are usually considered for secondary crystallization, namely, the formation of secondary crystals and lamellar thickening. Through extensive investigations of the secondary crystallization behavior of a number of polymers, Marand et al.[32−35] concluded that the predominant mechanism actually depends on the polymer architecture, the concentration of regio- and stereodefects, the sequence length distribution in random copolymers, the chain length and stiffness, and, most importantly, the crystallization temperature. In the case of poly(ether ether ketone), bisphenol A polycarbonate, isotactic polystyrene, and poly(ethylene terephthalate), they established that secondary crystallization typically occurs by secondary crystal formation below some critical temperature (defined as T_{co}), while above T_{co}, lamellar thickening is the dominant mechanism. These conclusions were consistent with results obtained on ethylene−octene copolymers for which secondary crystallization at low temperatures occurs by the mechanism of secondary crystal formation.

While the topic of secondary crystal formation in ethylene−styrene copolymers is addressed fully in the next paper of this series, we present here some preliminary evidence for the existence of a similar crossover from secondary crystal formation to lamellar thickening in the case of ESI-1.9. This evidence can be gathered in the present paper on the basis of data shown in Figures 1 and 3. Observation of a multiple melting behavior for ESI-1.9 and ESI-3.4 copolymers, similar to that reported earlier for ethylene/1-octene copolymers,[32] suggests that isothermal crystallization leads to the formation of two crystal populations of significantly different thermal stabilities. As in the case of ethylene/1-octene copolymers, we assign the low- and high-melting endotherms to the fusion of secondary and primary crystals, respectively. Evolutions of the low endotherm with crystallization time and temperature for ESI-1.9 and ESI-3.4 parallel that reported for ethylene/1-octene copolymers.[32] Increase in the low endotherm melting temperature with time is explained in terms of increasing topological constraints arising from the "cross-linking" of the remaining amorphous phase by small secondary crystals. No upward shifts of the *high* endotherm with crystallization time were observed in our previous investigations of ethylene/1-octene copolymers because crystallization temperatures were too low and comonomer contents generally too high. In the present study, the high endotherm peak temperature of ESI-1.9 (Figure 1e, f) and the intermediate endotherm peak temperature of ESI-3.4 (Figure 1g) increase with time at a rate $B(T_x)$, which is consistent with that exhibited by linear polyethylene and ESI-0.35 (Figure 3a). We will see below that such behavior is unambiguously explained in terms of isothermal lamellar thickening.

This qualitative picture of secondary crystallization is consistent with the observation (Figure 1) that increasing either the styrene content or the crystallization temperature leads to a larger ratio of low to high endotherm areas, i.e., a lower fraction of high-melting lamellar structures in samples crystallized for long

times. This picture is also consistent with the systematic weakening observed for the time dependence of the high endotherm melting temperature as the styrene content increases. Indeed, increasing the noncrystallizable comonomer content hinders the lamellar thickening process and favors secondary crystallization by secondary crystal formation, especially at the lowest temperatures. The rates, $B(T_x)$, at which high and low endotherm melting temperatures increase with time show dramatically different crystallization temperature dependences. This result parallels the results reported previously for it-PS, PEEK, and BAPC and supports our explanation of the multiple melting behavior in terms of the melting of primary crystals, which are of the chain folded lamellar type, and secondary crystals, which are of smaller lateral dimensions and possibly exhibit a lesser fraction of chain folding.

We now focus the remainder of this discussion on the behavior of linear polyethylene and ESI-0.35, which exhibit single melting endotherms, suggesting the existence of a unimodal distribution of crystals (Figure 1a−d). Previous morphological studies have established that these crystals are lamellar. The shift of the melting temperature with time under isothermal condition is observed over a wide range of crystallization temperatures (Figure 2). In addition, the increase in the rate of shift of the melting temperature, $B(T_x)$, with crystallization temperature indicates that the mechanism associated with the stabilization of lamellar crystals (increase in melting temperature) is a thermally activated process. These observations are consistent with the description of secondary crystallization in PE-119K and ESI-0.35 as a lamellar thickening process. Direct evidence for the lamellar thickening process was previously reported on the basis of Raman longitudinal acoustic mode and small-angle X-ray scattering studies.[36−41]

In a previous study[29] a quantitative model was developed to explain the correlation between the evolution of degree of crystallinity and that of the melting temperature for linear polyethylene. In that model lamellar thickening is assumed to follow a logarithmic law during isothermal crystallization. The increase in the melting temperature with time is accounted for by the intrinsic rate of lamellar thickening and by the rate of *primary* crystallization.

According to the DSC and temperature-modulated calorimetry results presented in Figures 4, 6, and 7, it is clear that the evolutions of the degree of crystallinity, melting temperature, and excess heat capacity are correlated during primary and secondary crystallization. Specifically, the excess heat capacity decay and the third stage of the melting temperature evolution can be unambiguously associated with secondary crystallization for both linear polyethylene (PE-119K) and the low styrene content ethylene copolymer (ESI-0.35).

In the first section we expand on these results[29] and interpret the secondary crystallization of linear polyethylene and ESI-0.35 at high temperature using the concept of chain-sliding and propose an indirect method for the determination of the associated activation energy using DSC and temperature-modulated calorimetry. In the second section the connections between secondary crystallization and reversible crystallization/melting during temperature modulation are discussed in detail in the context of the fold and lateral surface models.

Table 2. Apparent Activation Energy (E_a) for the Crystal α-Relaxation in Linear Polyethylene

	DS	DMA	solid-state NMR
E_a (kJ/mol)	106 (chlorinated PE)[46,47] 106 (oxidized HDPE)[47]	103[48]	122 ± 20[25,49]

1. Characterization of Lamellar Thickening. Lamellar thickening is believed to involve long-range cooperative chain -sliding in the crystalline regions, a process which is enabled by segmental jumps within the crystal lattice. The segmental jump process has been modeled initially by Mansfield et al.[42,43] and subsequently by Skinner et al.[44,45] using the soliton concept. The activation energy for the underlying crystal α_c-relaxation process (see Table 2) has been estimated through measurements of the relaxation time at different temperatures using techniques such as dielectric spectroscopy (DS),[46,47] dynamic mechanical analysis (DMA),[48] and solid-state NMR.[25,49]

We have shown in the previous section that the apparent activation energy associated with the decay of excess heat capacity is 94 ± 9 and 91 ± 10 kJ/mol for PE-119K and ESI-0.35, respectively. The values obtained for both samples are close to those listed in Table 2, suggesting that evolution of the excess heat capacity is likely to be controlled by the crystal α_c-relaxation process.

Here, it must be noted that the characteristic time τ in the KWW analysis was derived for relatively low crystallization temperatures (85−120 °C) where primary crystallization is complete at relatively short times. We noted earlier that the temperature dependence of $B(T_x)$ appears to become stronger above ca. 110 °C (Figures 3a). Loos et al.[50] monitored the evolution of the lamellar thickness for polyethylene using time-resolved SAXS/WAXS and longitudinal acoustic mode (LAM) Raman spectroscopy and reported a dramatic thickening during heating above 110 °C, which they attributed to a doubling of the lamellar thickness. Such a mechanism had been initially proposed by Barham et al.[51] on the basis of isothermal crystallization studies at high temperature. Subsequent time-resolved SAXS studies by Bark et al.[52] and Albrecht et al.,[53] however, failed to confirm any discontinuous change in the long period during isothermal crystallization. We should therefore ask whether the evolution of the melting temperature ($B(T_x)$) follows different mechanisms at low and high temperatures.

To shed further light on this issue, it is essential to find other methods for the direct or indirect characterization of the lamellar thickening process in as wide a temperature range as feasible. We suggest that $B(T_x)$ is possibly a good candidate, considering that it can be obtained at quite high crystallization temperatures. Arrhenius plots for $B(T_x)$ are shown in Figure 9. The Arrhenius plots for τ are also included in Figure 9a and b as a comparison. Our analysis indicates that the temperature dependence of $B(T_x)$ is very well described by a single Arrhenius equation over the whole temperature range and that *no crossover* is observed at ca. 110 °C. Additionally, the apparent activation energy calculated from Arrhenius plots for $B(T_x)$ is relatively close to that obtained from τ (see Table 3). This further supports our speculation that $B(T_x)$, the rate of change of the melting temperature, is controlled by the same underlying molecular mechanism, i.e., the crystal α_c-relaxation.

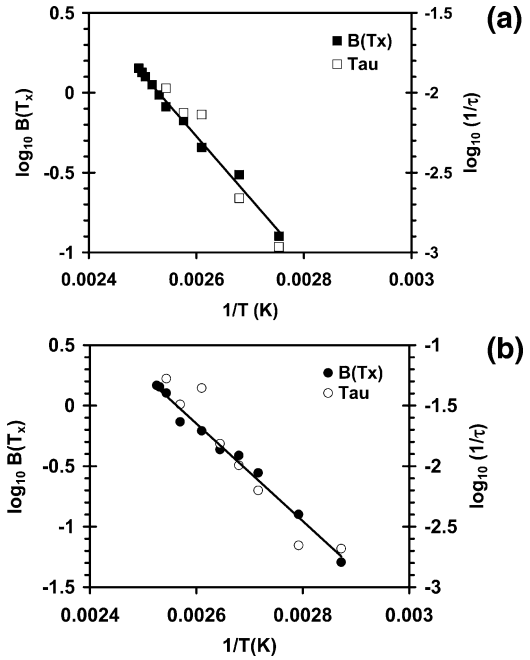

Figure 9. Comparisons of Arrhenius plots for $B(T_x)$ and τ for (a) PE-119K and (b) ESI-0.35.

Table 3. Apparent Activation Energy Estimated from the Temporal Evolutions of the Excess Heat Capacity and Melting Temperature for Crystallization at Different Temperatures

	E_a (kJ/mol)	
samples	from τ	from B
PE-119K	94 ± 9	75 ± 3
ESI-0.35	91 ± 10	78 ± 3

Considering Figure 3a, one might be surprised that the curve $B(T_x)$ shows little or no dependence on the styrene content (in the range from 0 to 3.4 mol %) for temperatures below 110 °C. If this is indeed so, then the thickening rate should be expected to depend little on the comonomer content. We can rationalize this observation as follows. At lower crystallization temperatures lamellae are thinner. Under these conditions the lamellar thickness may not be affected significantly by the copolymer sequence length distribution and should be primarily controlled by the undercooling. Hence, one could anticipate that a certain amount of thickening can take place before the constraints associated with noncrystallizable units are felt. Second, but equally important, is the fact that the rate of thickening decreases with decreasing temperature. Hence, as the temperature is lowered, thickening can no longer occur on large length scales but is likely to become a more local process. Hence, the effect of styrene content on the thickening of lamellar crystals is not likely to be observed at the early stages of thickening but is predicted to eventually set in as the extent of thickening increases and the constraints associated with the localization of styrene units at the crystal melt interface are felt.

Within the uncertainty of the measurements and the analysis, we do not observe any dependence of the comonomer content on the activation energy. Examination of Figure 9a indeed shows that the best fit line for $\log B$ vs $1/T_x$ describes very well the Arrhenius plot for $\log \tau$, while a 20% difference in activation energy (Table 3) might be inferred from the respective linear regressions.

We note that others have used a linear combination of two exponential functions to fit the time evolution of the reversing heat capacity[7,9,12,54]

$$C_p^{rev}(t) = C_p^{rev}(\infty) + a_1 e^{-t/\tau 1} + a_2 e^{-t/\tau 2} \qquad (7)$$

This approach suggests the existence of two processes with characteristic time τ_1 and τ_2 contributing to the decay of excess heat capacity. According to these authors the fast process is associated with secondary crystallization while the slow process, with a time constant on the order of 100 min, is thought to relate to some relaxation process. Considering the temperature dependence of secondary crystallization rates and chain dynamics, systematic changes in τ_1 and τ_2 with temperature were expected. We therefore attempted to fit our excess heat capacity data using eq 7. No obvious trends in either τ_1 or τ_2 as a function of crystallization temperature were found. We note that in a recent study on ultrahigh molar mass polyethylene, Höhne et al.[55] also used eq 7 to fit the excess heat capacity data. In their case, τ_1 (the shorter time) shows a systematic dependence on temperature in the 90−120 °C range, but their estimated τ_2 values are scattered, making the subsequent Arrhenius analysis impossible.

Finally, we note that previous TMDSC experiments by Schick and collaborators[56−58] have shown that the excess heat capacity decreases with increasing modulation frequency. At sufficiently high modulation frequency there is insufficient time for reversible crystallization/melting events to take place. It will be worthwhile for future experiments to probe the influence of modulation frequency on the shape of the excess heat capacity decay curve and on the calculated activation energy.

2. Mechanism of Reversible Crystallization and Melting−Fold or Lateral Surface Processes? As mentioned in the Introduction, two competing models were proposed to explain the generation of excess heat capacity. Although these two models differ as to the site of reversible crystallization and melting, both models emphasize the existence of a balance between crystallization and entropic forces. In the fold surface model the crystallization force tends to pull segments into the crystalline phase, thus leading to the enhanced elastic force exerted on the amorphous chain. In the lateral surface model the crystallization force leads to the localization and attachment of polymer segments on the lateral surface of existing crystallites, thus leading again to an enhanced elastic force on the remaining amorphous chains. Which process takes place depends on the crystallization conditions and the polymer microstructure. Chain sliding in the crystalline phase is expected to be favored at high temperatures, where the constraints in the interlamellar amorphous fraction and at the crystal fold surface are minimized. Hence, lower chain length[59] (i.e., fewer entanglements) and lower noncrystallizable comonomer content favor high sliding efficiency and thus the fold−surface model. A decrease in thickening rate with increasing chain length has indeed been reported for linear polyethylene fractions by Mandelkern et al.[41]

We first note that during primary crystallization the excess heat capacity is directly proportional to the degree of crystallinity as shown in parts a and b of Figure 7. Second, the onset of secondary crystallization is associated with the departure from proportionality between these quantities. Finally, as shown in Figure

6, the decay in excess heat capacity occurs over the same time scale as the final stage of the melting temperature evolution (pure secondary crystallization). These observations allow us to conclude that the excess heat capacity discussed in regard to Figures 5−8 is a characteristic property of as-formed primary lamellar crystals. These results also suggest that some of the molecular processes which enable lamellar thickening also lead to a steady and systematic decrease in the reversible latent heat effects. The important observation that *secondary crystallization by lamellar thickening and reversibility of the latent heat effects are correlated in the time domain suggests very strongly that the reversible crystallization/melting phenomenon is associated with molecular events in the melt−crystal fold interfacial region*. With this conclusion in hand, we can now rationalize the evolution of the excess heat capacity during crystallization.

Polymer chains at the melt−crystal interface are in a local but not a global equilibrium state. On a long time scale thickening can lead to a decrease in the specific surface area of lamellar crystals and thus lower their free energy. On a shorter time scale we can consider that polymer chains in the crystal−liquid interphase are in a state of local equilibrium. As a first-order approximation, we may consider that small temperature oscillations during the quasi-isothermal calorimetric measurements simply lead to an in-phase oscillation in the position of this local equilibrium. The nature of this local equilibrium has been previously discussed by Fischer et al.,[21,24] Mansfield et al.,[22,23] and Strobl et al.[8,16,20] During one period of the temperature oscillation chain segments in the fold crystal−liquid interphase are successively pulled in and out of the crystals as a result of the temperature-dependent balance between crystallization and elastic forces. During primary crystallization the systematic increase in the crystal volume fraction leads to a parallel increase in the number of chains that participate in the reversible crystallization−melting process. Proportionality between these two quantities (X_c and C_p^{exc}) will only be maintained as long as the change in crystallinity occurs by a single mechanism. Toward the end of the primary crystallization stage the number of lamellae approaches an asymptotic value. Hence, we would expect the excess heat capacity to reach a similar plateau. At the same time as the change in primary crystallinity becomes vanishingly small, secondary crystallization (lamellar thickening) starts to contribute more significantly to the change in crystallinity. As the crystallization process transitions from the primary to the secondary stage, one would therefore expect the excess heat capacity, C_p^{exc}, to become constant and the ratio C_p^{exc}/X_c to start decreasing. Figure 7 indeed confirms that this ratio starts decreasing at the same time as the pure primary crystallization regime ends (end of the Avrami regime and onset of the second stage of the melting temperature evolution). On the other hand, Figure 5 clearly indicates that C_p^{exc} does not reach a plateau but rather a maximum in the intermediate or mixed stage. During secondary crystallization C_p^{exc} exhibits a continuous decay at a rate (given by $1/\tau(T_x)$) which increases with secondary crystallization temperature. Furthermore, the rate of decay of C_p^{exc} parallels the rate of *secondary crystallization*. This important conclusion is reached when noting that $\tau(T_x)$ and $B(T_x)$ exhibit similar temperature dependences (Figure 9) and recalling from our earlier studies[29] that the rate of secondary crystallization controls the temporal evolution of the melting temperature, as given by $B(T_x)$.

The decrease in C_p^{exc} must therefore reflect the evolution of a molecular property that is associated with the lamellar thickening process. We speculate that as secondary crystallization proceeds, loops and tie-chains in the crystal−liquid interphase become systematically more constrained and display reduced ability to undergo the reversible crystallization−melting event associated with the temperature modulation. According to this qualitative description, the time scale associated with the decay of the excess heat capacity should be comparable to the time scale associated with the constraining of loops and tie-chains, thus with the characteristic time scale for the thickening process. Since the latter is believed to be controlled by the segmental jump rate in the crystal phase (α_c relaxation), one should therefore not be surprised that the apparent activation energies derived in Table 3 from the temperature dependences of $1/\tau(T_x)$ or $B(T_x)$ are indeed very close to that reported for the α_c relaxation (Table 2).

Calculating the reversible fraction of the latent heat, Goderis et al.[15] showed that the reversible attachment/detachment process on the lateral surface of a lamella cannot account for the magnitude of the excess heat capacity. With support from this simple calculation, we conclude that the contribution to the excess heat capacity from reversible attachments/detachments on lateral lamellar surfaces is likely to be negligible, even if it exists. At the same time, Goderis's calculation suggests that reversible crystallization and melting on the lateral surfaces of *small* crystallites is only a likely mechanism in the case of high styrene content copolymer. Indeed, small crystallites have a considerably larger specific surface area than large crystals. This issue will be addressed further in the following paper.

We therefore anticipate that both the fold and the lateral surface models of reversible latent heat effects are relevant for polymer crystallization, albeit in different temperature ranges and for different crystal morphologies. This reconciled view of reversible latent heat effects in semicrystalline polymers is fully consistent with our general description of secondary crystallization.

Conclusions

Using a combination of differential scanning calorimetry and quasi-isothermal temperature-modulated calorimetry, we investigated the temporal evolutions of the melting temperature, degree of crystallinity, and excess heat capacity during crystallization of linear polyethylene and low styrene content ethylene−styrene copolymers. Describing isothermal crystallization as the succession of three stages (primary, mixed, and secondary crystallization stages), we established the following correlations: (1) the evolution of the melting temperature with time parallels that of the degree of crystallinity, (2) the excess heat capacity increases linearly with degree of crystallinity during the primary stage, reaches a maximum during the mixed stage, and decays during the secondary stage, (3) the rate of decay of the excess heat capacity parallels the rate of secondary crystallization, and (4) the rates of shift of the melting temperature and decay of the excess heat capacity lead to apparent activation energies that are very similar to these reported for the crystal α_c relaxation by solid-state

NMR, dynamic mechanical, and dielectric spectroscopies. Strong correlations in the time domain for secondary crystallization by lamellar thickening and evolution of the excess heat capacity suggest that the reversible crystallization/melting phenomenon is associated with molecular events in the melt−crystal fold interfacial region.

Specifically, we conclude that the excess heat capacity observed during the high-temperature crystallization of linear polyethylene and low styrene content copolymers is most likely to originate from the segmental processes in the crystal/melt fold region that have been discussed by Fischer, Mansfield, and Strobl. These studies also provide preliminary indications that the excess heat capacity observed during crystallization at lower temperatures in the case of ethylene copolymers of high comonomer content is consistent with the lateral surface model proposed by Wunderlich.

Acknowledgment. We (H.M. and Z.H.) thank the Dow Chemical Co. for the supply of materials as well as for the support of this research.

References and Notes

(1) Marand, H.; Xu, J.; Srinivas, S. *Macromolecules* **1998**, *31*, 8219.
(2) Toda, A.; Oda, T.; Hikosaka, M.; Saruyama, Y. *Thermochim. Acta* **1997**, *293*, 47.
(3) Okazaki, I.; Wunderlich, B. *Macromolecules* **1997**, *30*, 1758.
(4) Ishikiriyama, K.; Wunderlich, B. *Macromolecules* **1997**, *30*, 4126.
(5) Ishikiriyama, K.; Wunderlich, B. *J. Polym. Sci., Part B: Polym. Phys.* **1997**, *35*, 1877.
(6) Wurm, A.; Merzlyakov, M.; Schick, C. *Colloid Polym. Sci.* **1998**, *276*, 289.
(7) Androsch, R.; Wunderlich, B. *Macromolecules* **1999**, *32*, 7238.
(8) Hu, W.; Albrecht, T.; Strobl, G. *Macromolecules* **1999**, *32*, 7548.
(9) Pyda, M.; Wunderlich, B. *J. Polym. Sci., Part B: Polym. Phys.* **2000**, *38*, 622.
(10) Wurm, A.; Merzlyakov, M.; Schick, C. *J. Therm. Anal.* **2000**, *60*, 807.
(11) Androsch, R.; Wunderlich, B. *Macromolecules* **2000**, *33*, 9076.
(12) Pak, J.; Wunderlich, B. *Macromolecules* **2001**, *34*, 4492.
(13) Androsch, R.; Wunderlich, B. *Macromolecules* **2001**, *34*, 8384.
(14) Albrecht, T.; Armbruster, S.; Keller, S.; Strobl, G. *Macromolecules* **2001**, *34*, 8456.
(15) Goderis, B.; Reynaers, H.; Scherrenberg, R.; Mathot, V. B. F.; Koch, M. H. J. *Macromolecules* **2001**, *34*, 1779.
(16) Albrecht, T.; Armbruster, S.; Keller, S.; Strobl, G. *Eur. Phys. J. E.*6 **2001**, 237.
(17) Androsch, R.; Wunderlich, B. *Macromolecules* **2001**, *34*, 5950.
(18) Pak, J.; Wunderlich, B. *J. Polym. Sci., Part B: Polym. Phys.* **2002**, *40*, 2219.
(19) Wunderlich, B. *Prog. Polym. Sci.* **2003**, *28*, 383.
(20) Albrecht, T.; Strobl, G. *Macromolecules* **1995**, *28*, 5827.
(21) Fischer, E. W. *Kolloid Z. Z. Polym*. **1967**, *218*, 97.
(22) Mansfield, M. L. *Macromolecules* **1987**, *20*, 1384.
(23) Rieger, J.; Mansfield, M. L. *Macromolecules* **1989**, *22*, 3810.
(24) Tanabe, Y.; Strobl, G. R.; Fischer, E. W. *Polymer* **1986**, *27*, 1147.
(25) Hu, W.-G.; Boeffel, C.; Scmidt-Rohr, K. *Macromolecules* **1999**, *32*, 1611.
(26) Androsch, R.; Moon, I.; Kreitmeier, S.; Wunderlich, B. *Thermochim. Acta* **2000**, *357*−*358*, 267.
(27) Advanced Thermal Analysis System (ATHAS) data bank. See http://web.utk.edu/~athas.
(28) See http://ois.nist.gov/srmcatalog/certificates/view_cert2gif.cfm?certificate=720.
(29) Marand, H.; Huang, Z. Y. *Macromolecules* **2004**, *37*, 6492.
(30) Mandelkern, L. In *Crystallization of Polymers*; McGraw-Hill: New York, 1962.
(31) Schick, C.; Merzlyakov, M.; Wunderlich, B. *Polym. Bull.* **1998**, *40*, 297.
(32) Alizadeh, A.; Richardson, L.; Xu, J.; McCartney, S.; Marand, H.; Cheung, Y. W.; Chum, S. *Macromolecules* **1999**, *32*, 6221.
(33) Marand, H.; Alizadeh, A.; Farmer, R.; Desai, R.; Velikov, V. *Macromolecules* **2000**, *33*, 3392.
(34) Alizadeh, A.; Sohn, S.; Quinn, J.; Marand, H.; Shank, L. C.; Iler, H. D. *Macromolecules* **2001**, *34*, 4066.
(35) Marand, H.; Alizadeh, A.; Sohn, S.; Xu, J.; Farmer, R.; Prabhu, V.; Cronin, S.; Velikov, V. *Antec 2001 Proc.* **2001**, *#0051* (Vol. III), 856.
(36) Fischer, E. W.; Schmidt, G. F. *Angew. Chem., Int. Ed.* **1962**, *1* (9), 448.
(37) Weeks, J. J. *J. Res. Natl. Bur. Stand.* **1963**, *67A*, 441.
(38) Hoffman, J. D. *Soc. Plast. Eng. Trans.* **1964**, *4*, 315.
(39) Fischer, E. W. *Pure Appl. Chem.* **1972**, *31*, 113.
(40) Duglosz, J.; Fraser, G. V.; Grubb, D.; Keller, A.; Odell, J. A.; Goggin, P. L. *Polymer* **1976**, *17*, 479.
(41) Stack, G. M.; Mandelkern, L.; Voigt-Martin, I. G. *Polym. Bull.* **1982**, *8*, 421.
(42) Mansfield, M.; Boyd, R. H. *J. Polym. Sci., Polym. Phys. Ed.* **1978**, *16*, 1227.
(43) Mansfield, M. L. *Chem. Phys. Lett.* **1980**, *69*, 383.
(44) Skinner, J. L.; Wolynes, P. G. *J. Chem. Phys.* **1980**, *73*, 4015.
(45) Skinner, J. L.; Park, Y. H. *Macromolecules* **1984**, *17*, 1735.
(46) Aschcraft, C. R.; Boyd, R. H. *J. Polym. Sci., Polym. Phys. Ed.* **1976**, *14*, 2154.
(47) Graff, M. S.; Boyd, R. H. *Polymer* **1994**, *35*, 1797.
(48) McCrum, N. G.; Read, B. E.; Williams, G. *Anelastic and Dielectric Effects in Polymeric Solids*; Dover Publications: New York, 1991.
(49) Hu, W. G.; Boeffel, C.; Schmidt-Rohr, K. *Macromolecules* **1999**, *32*, 1714.
(50) Loos, J.; Tian, M.; Rastogi, S.; Lemstra, P. J. *J. Mater. Sci.* **2000**, *35*, 5147.
(51) Barham, P. J.; Keller, A. *J. Polym. Sci. Polym. Phys. Ed.* **1989**, *27*, 1029.
(52) Bark, M.; Zachmann, H. G.; Alamo, R.; Mandelkern, L. *Makromol. Chem.* **1992**, *193*, 2363.
(53) Albrecht, T.; Strobl, G. *Macromolecules* **1996**, *29*, 783.
(54) Di Lorenzo, M. L.; Pyda, M.; Wunderlich, B. *J. Polym. Sci., Part B: Polym. Phys.* **2001**, *39*, 2969.
(55) Höhne, G. W. H.; Kurelec, L.; Rastogi, S. *Thermochim. Acta* **2003**, *396*, 97.
(56) Schick, C.; Wurm, A.; Mohammed, A. *Colloid Polym. Sci.* **2001**, *279*, 800.
(57) Schick, C.; Wurm, A.; Merzlyakov, M.; Minakov, A.; Marand, H. *Macromol. Symp.* **2001**, *165*, 83.
(58) Schick, C.; Wurm, A.; Mohammed, A. *Thermochim. Acta* **2003**, *396*, 119.
(59) The chains are nevertheless assumed to be long enough that the lamellar crystals are chain folded (i.e., this discussion is not concerned with short paraffins which form extended chain crystals that do not thicken. These latter materials will most likely undergo reversible crystallization on the lateral crystal surfaces as pointed out by Pak and Wunderlich[12]).

MA049411G